



Improvements to the photocatalytic efficiency of polyaniline modified TiO_2 nanoparticles

M. Radoičić^a, Z. Šaponjić^a, I.A. Janković^a, G. Čirić-Marjanović^b, S.P. Ahrenkiel^c, M.I. Čomor^{a,*}

^a Vinča Institute of Nuclear Sciences, University of Belgrade, P.O. Box 522, 11001 Belgrade, Serbia

^b Faculty of Physical Chemistry, University of Belgrade, Studentski Trg 12–16, 11158 Belgrade, Serbia

^c South Dakota School of Mines & Technology, USA

ARTICLE INFO

Article history:

Received 5 November 2012

Received in revised form

31 December 2012

Accepted 4 January 2013

Available online 16 January 2013

Keywords:

Photocatalysis

TiO_2

Polyaniline

ABSTRACT

Polyaniline/ TiO_2 nanocomposite powders were successfully synthesized by the oxidative polymerization of aniline with ammonium peroxydisulfate in water without the addition of acid, in the presence of colloidal TiO_2 nanoparticles ($d \sim 4.5$ nm). The morphological, structural, and optical properties of the synthesized nanocomposites prepared at initial TiO_2 /aniline mole ratios of 50, 100, and 150 were studied using transmission electron microscopy, X-ray powder diffraction, Raman and UV-vis spectroscopies. The presence of emeraldine salt and the base form of linear polyaniline (PANI) chains as well as the presence of phenazine units, branched PANI chains, oligomeric structures and short PANI chains in PANI/ TiO_2 nanocomposites was confirmed by Raman spectroscopy. The anatase crystal structure of TiO_2 nanoparticles in all the nanocomposites was confirmed by X-ray powder diffraction measurements and by Raman spectroscopy. The photocatalytic activities of PANI/ TiO_2 nanocomposites were evaluated using the photocatalytic degradation of Rhodamine B and Methylene blue as model compounds and compared with the activity of bare colloidal TiO_2 nanoparticles. Enhanced degradation efficiencies in the dyes used were observed. A possible explanation for the PANI/ TiO_2 photocatalytic activities was suggested, taking into account the influence of the molecular structures of the used dyes and PANI in PANI/ TiO_2 nanocomposites.

© 2013 Elsevier B.V. All rights reserved.

1. Introduction

TiO_2 as a wide band gap ($E_g = 3.2$ eV) inorganic semiconductor is a promising material for photoelectric conversion and the photocatalytic treatment of pollutants in water and air, due to its reasonably good photocatalytic activity under ultraviolet (UV)-light irradiation ($\lambda < 380$ nm), its photostability and its nontoxicity [1]. It is well known that the photocatalytic activity of TiO_2 is governed by various factors such as surface area, phase structure, interfacial charge transfer, and the separation efficiency of photoinduced electrons and holes [2]. However, the poor response within the visible-light spectral range strongly limited the application of TiO_2 materials. In order to use solar energy more efficiently, many groups have reported the usage of organic dyes as photosensitizers, especially in the field of solar cells [3–5]. These molecules are able to absorb visible light photons and inject electrons to the conduction band (CB) of TiO_2 .

The high absorption coefficients in the visible part of the spectrum, high mobility of charge carriers (a consequence of the

extended π -conjugated electronic system) and good environmental stability of conductive polymers mean they are a good choice for TiO_2 sensitization. Moreover, many conductive polymers, in both their doped and undoped states, are efficient electron donors and good hole transporters upon visible light excitation [6]. Recently, some studies have reported on the combination of PANI and TiO_2 with the aim of improving their performance in relation to UV light or sunlight activity [7–10]. This is to be expected, bearing in mind that polyaniline (PANI) is a conducting polymer and a dye with a forbidden band gap of 2.8 eV [11], making it a good sensitizer of TiO_2 . In addition, TiO_2 is an n-type semiconductor while PANI can behave as a p-type semiconductor [12]. Xiong et al. synthesized PANI/ TiO_2 bilayer microtubes by a two-step process using anodic aluminum oxide as a template, and detected enhanced photocatalytic activity under sunlight in comparison with bare TiO_2 microtubes [7]. Zhang et al. synthesized nanocomposite powders with different PANI: TiO_2 ratios using commercial anatase TiO_2 powder as a precursor. They followed weight loss of PANI deposited on TiO_2 surface as a function of irradiation time [8]. Li et al. have formed a self-assembled monolayer (SAM) of γ -aminopropyltriethoxysilane on the surface of TiO_2 nanoparticles (NPs) that provided a further surface oxidative graft polymerization to form a dense PANI layer. They compared the photocatalytic activity of bare- TiO_2

* Corresponding author. Tel.: +381 113408192.

E-mail address: mirjanac@vinca.rs (M.I. Čomor).

NPs with the PANI/SAM-TiO₂ nanocomposites following the photodegradation of methyl orange under sunlight [9]. Recently, the photocatalytic degradation of methylene blue over PANI/TiO₂ nanocomposites has been obtained by mixing commercial TiO₂ nanopowders (for example Degussa) and PANI synthesized by the chemical oxidative polymerization [10,13,14]. Li et al. synthesized PANI/TiO₂ nanocomposites by the chemical oxidative polymerization of aniline in the presence of powdered TiO₂ NPs. They noticed that the presence of PANI molecules (in emeraldine salt form) on the TiO₂ surface could prevent aggregation, and at the same time sensitize TiO₂ NPs, which thus provide better photocatalytic activity for PANI/TiO₂ nanocomposites in comparison with bare TiO₂ NPs [6,15]. Also, PANI/TiO₂ films were prepared using different methods, with or without templates, again showing improved photocatalytic activity compared to bare TiO₂ [16–18].

The subject of this work was the *in situ* synthesis, characterization and systematic study of the photocatalytic activity of various PANI/TiO₂ nanocomposites. In order to obtain information about their molecular and crystalline structure, as well as the morphology of the PANI layer, synthesized nanocomposites were characterized by various techniques, such as, Raman and UV-vis spectroscopies, X-ray powder diffraction (XRD) and transmission electron microscopy (TEM). The potential applicability of synthesized PANI/TiO₂ nanocomposites as a photocatalysts was checked following the photodegradation reaction of model compounds: methylene blue (MB) and Rhodamine B (RB) in a suspension. To the best of our knowledge, the synthesis of colloidal aqueous dispersion of photocatalytic active PANI/TiO₂ nanocomposite materials, without the addition of any acid and/or surfactant and their systematic study, are presented here for the first time.

2. Experimental

2.1. Materials

All chemicals were reagent-grade and used as received (Aldrich, Fluka), except aniline (ANI). Aniline (p.a., >99.5%, Centrohem, Serbia), was distilled under reduced pressure and stored at room temperature, under argon, prior to use. Ammonium peroxydisulfate (APS) (analytical grade, Centrohem, Serbia) was used as received. Milli-Q deionized water was used as a solvent.

2.2. Synthesis of colloidal TiO₂ NPs

The colloidal solution of TiO₂ NPs was prepared in a manner analogous to the procedure proposed by Rajh et al. [19]. The TiCl₄ cooled to –20 °C was added drop-wise to cooled water (at 4 °C) under vigorous stirring and then kept at this temperature for 30 min. The pH value of the solution was between 0 and 1, depending on the TiCl₄ concentration. The slow growth of the particles was achieved by applying dialysis against water at 4 °C until the pH of the solution reached 3.5. The Spectra/Por Dialysis Membrane, MWCO: 3500 (Spectrum Laboratories, Inc., Rancho Dominguez, CA) was used for the dialysis of the colloidal solution. The concentration of TiO₂ was determined from the concentration of the peroxide complex obtained after dissolving the particles in concentrated H₂SO₄ [20].

2.3. Synthesis of PANI/TiO₂ nanocomposites

In a typical procedure for preparing PANI in the presence of TiO₂ NPs, the aqueous solutions of ANI, oxidant (APS), and colloidal TiO₂ NPs were mixed at room temperature. The PANI/TiO₂ nanocomposites prepared at initial [TiO₂]/[ANI] mole ratios of 50, 100 and 150 and initial mole ratio [APS]/[ANI] = 1.25 are designated

as TP-50, TP-100 and TP-150, respectively. Due to the low concentration of ANI, the reaction mixture was stirred for 20 days. In order to remove residual monomer, oxidant and low-molecular weight fractions, PANI/TiO₂ composite was dialyzed in Milli-Q deionized water. Finally, the nanocomposites were dried in a vacuum oven at 60 °C until a constant mass was reached. Dry colloidal TiO₂ powder was used as a reference sample.

2.4. Characterization

Raman spectra excited by a diode-pumped solid-state laser (at an excitation wavelength of 532 nm) were collected on a Thermo Scientific DXR Raman microscope, equipped with a research optical microscope and a CCD detector. The laser beam was focused on the sample placed on an X-Y motorized sample stage using an objective magnification of 50×. The scattered light was analyzed by the spectrograph with a 900 lines mm^{–1} grating. Laser power was in a range from 0.5 mW to 9 mW.

UV-vis and reflectance spectra of pure TiO₂ NPs and PANI/TiO₂ nanocomposite samples were obtained using an Evolution 600 spectrophotometer (Thermo Scientific).

The XRD powder patterns were obtained by using a Philips PW 1050 powder diffractometer with Ni filtered Cu K_α radiation ($\lambda = 1.5418 \text{ \AA}$). The diffraction intensity was measured by the scanning technique (a step size of 0.05° and a counting time of 50 s per step).

TEM images obtained on a Hitachi H-7000 FA TEM operated at 125 kV, were used to determine the sizes of the TiO₂ NPs and the thickness of the PANI layer on the surface of TiO₂ NPs.

2.5. Photocatalytic activity test

The photocatalytic activities of the prepared samples were evaluated following the degradation of RB and MB in an aqueous solution. 50 mL of dye aqueous solution with a concentration of $1 \times 10^{-5} \text{ mol L}^{-1}$ was mixed with 1 g L^{–1} of catalyst (PANI/TiO₂ or neat colloidal TiO₂). Suspensions were placed into a vessel which was exposed to white light from an Osram Vitalux lamp (300 W, Sun light simulation, white light: UVB radiated power from 280 to 315 nm 3.0 W; UVA radiated power 315–400 nm 13.6 W; the rest is visible light and IR). Optical power was measured using R-752 Universal Radiometer read out with sensor model PH-30, DIGIRAD and it was $\sim 30 \text{ mW cm}^{-2}$ at a distance of 30 cm from experimental solutions (used in this study). Before irradiation, the suspensions were stirred for at least 15 min in the dark to establish an adsorption–desorption equilibrium. Samples were saturated with oxygen and stirred during the irradiation. Aliquots of 1 mL were taken out from the suspensions every 60 min during the irradiation. The photocatalyst was separated from the solution by centrifugation and the absorbance intensities of the dyes, RB and MB in the supernatant were measured at $\lambda = 554 \text{ nm}$ and $\lambda = 664 \text{ nm}$, respectively (Evolution 600 spectrophotometer – Thermo Scientific). The molecular structures of used dyes are shown in Fig. 6 as insets.

3. Results and discussion

3.1. Structural and optical characterization of PANI/TiO₂ nanocomposites

The characteristic bands in Raman spectra of TP-50, TP-100 and TP-150 nanocomposites, shown in Fig. 1, confirmed the presence of anatase TiO₂ NPs in all the samples. The characteristic Raman bands of anatase structure [21–23] were observed at wavenumbers 151, 206 and 644 cm^{–1} for the TP-50 nanocomposite, at 154, 205 and 629 cm^{–1} for the TP-100 nanocomposite, and at 153, 203, 510 and 627 cm^{–1} for the TP-150 nanocomposite.

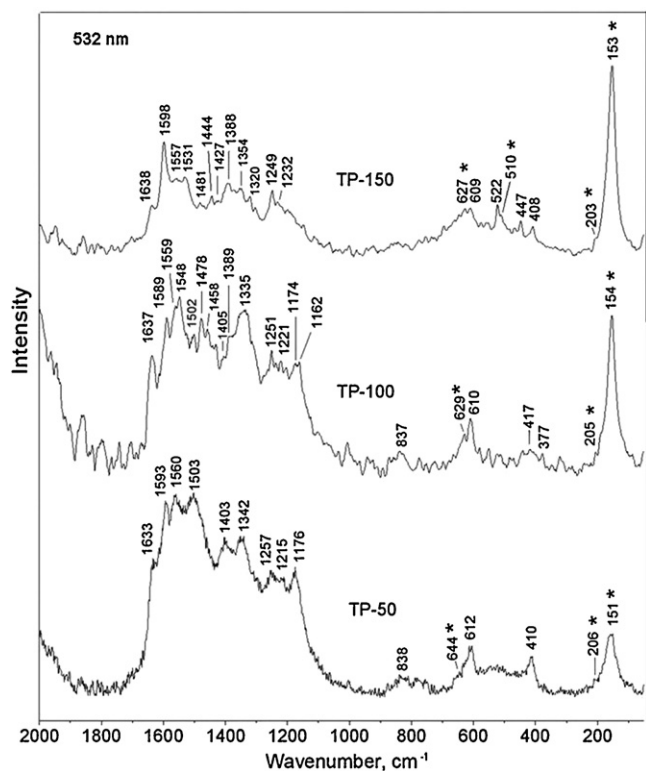


Fig. 1. The Raman spectra of TP-50, TP-100 and TP-150 nanocomposites; $\lambda_{\text{exc}} = 532 \text{ nm}$. The bands marked with an asterisk are assigned to anatase TiO_2 .

In the spectrum of the TP-50 nanocomposite (Fig. 1) the Raman bands assigned to PANI chains in their emeraldine salt (ES) form were observed at 1593 cm^{-1} (the $\text{C}=\text{C}$ and $\text{C}\sim\text{C}$ stretching vibrations of the quinonoid (Q) and/or semiquinonoid (SQ) rings, respectively, where \sim denotes the bond intermediate between the single and double bond), 1503 cm^{-1} (the $\text{N}-\text{H}$ bending vibration of protonated amine), 1342 cm^{-1} (the $\text{C}\sim\text{N}^+$ stretching vibration of polaronic structures), and 1176 cm^{-1} (the $\text{C}-\text{H}$ bending in-plane vibration of SQ rings in polaronic structures) [24]. In the spectrum of the TP-100 nanocomposite, these bands characteristic of the ES form are red-shifted compared to those observed in the spectrum of the TP-50 sample and appeared at 1589 , 1502 , 1335 , and 1174 cm^{-1} . Additional bands ascribed to the vibrations of Q rings can also be seen in the spectrum of the TP-100 sample at 1162 cm^{-1} (the $\text{C}-\text{H}$ bending in-plane vibration of Q rings), and again at 1478 and 1458 cm^{-1} (the $\text{C}=\text{N}$ stretching vibrations of various types of Q rings). The presence of the bands at $\sim 1160 \text{ cm}^{-1}$ and $\sim 1480 \text{ cm}^{-1}$, characteristic of the PANI emeraldine base (EB) form [24], is an indication of the lower level of protonation of PANI chains, and consequently the lower conductivity of PANI in the TP-100 sample.

Along the bands of ordinary PANI, bands which have been associated with the substituted phenazine units [24] were also observed at 1633 , 1560 and 1403 cm^{-1} for the TP-50 sample, at 1637 , 1559 , 1548 , 1405 , and 1389 cm^{-1} for the TP-100 sample, and at 1638 , 1557 , 1531 , 1427 , and 1388 cm^{-1} for the TP-150 sample. These types of structural units were found to be very important in the formation of PANI nanostructures *via* the self-assembly process, as shown by the template-free falling-pH method [24–27].

The relative intensity of the TiO_2 bands increases with increase of the TiO_2 content in the nanocomposite (Fig. 1). It should be noted that the band at 1559 cm^{-1} (the phenazine band) is stronger than that at 1589 cm^{-1} (the Q band) in the spectrum of TP-100, while in the spectrum of TP-150 the band at 1598 cm^{-1} due to the $\text{C}=\text{C}$ stretching vibrations of Q rings becomes the dominant band,

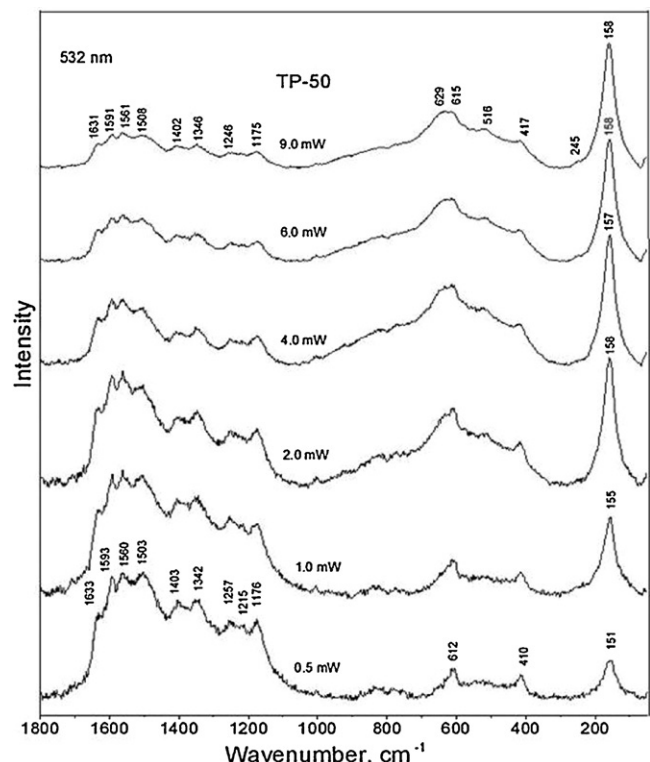


Fig. 2. The Raman spectra of TP-50 nanocomposite recorded at different laser powers from 0.5 mW to 9.0 mW ; $\lambda_{\text{exc}} = 532 \text{ nm}$.

and is much stronger than the band at 1557 cm^{-1} . The low conductivity of PANI chains in TP-150 is indicated by the absence of bands at $\sim 1176 \text{ cm}^{-1}$ and $\sim 1503 \text{ cm}^{-1}$ of conducting ES form in the Raman spectrum. The spectral pattern of the organic part of the TP-150 composite resembles more closely the spectrum of branched oligomers of N-C2 coupled ANI dimer [28] than the spectrum of ordinary PANI-ES. The increased intensity of the band at 1598 cm^{-1} may originate from the terminal units in short chains.

It is important to note that PANI in nanocomposites is very resistant to the degradation induced by the laser power applied in the Raman spectroscopy measurements, as shown in the example of TP-50 (Fig. 2). Here, when the laser power was gradually increased from 0.5 mW to 9.0 mW (Fig. 2) the PANI bands in the spectrum of TP-50 became weaker in relation to the TiO_2 bands, but the carbonization of PANI was not detected. The degradation of PANI chains was suppressed by the presence of a substantial quantity of thermally resistant TiO_2 NPs. We have recently demonstrated that when the nanocomposites contained significantly lower amounts of TiO_2 ($\text{ANI}:\text{TiO}_2 = 20:1$), the applied laser power of 2.0 mW produced the carbonization of PANI chains and the PANI spectral pattern was transformed into only two broad bands at $\sim 1570 \text{ cm}^{-1}$ and 1350 cm^{-1} , which is typical of carbonized PANI [29].

The UV/Vis reflectance spectra of the colloidal TiO_2 NPs and PANI/ TiO_2 nanocomposites are shown in Fig. 3. It can be seen that both TiO_2 NPs and PANI/ TiO_2 nanocomposites absorb light below 400 nm . Above this wavelength, only nanocomposites absorb light showing the band at $\sim 440 \text{ nm}$, accompanied by the broad band in the range of 500 – 700 nm . The band at $\sim 440 \text{ nm}$ is characteristic of conducting PANI-ES, ascribed to the polaron $\rightarrow \pi^*$ transition [29,30].

The typical $\pi \rightarrow \text{polaron}$ band of fully protonated PANI-ES usually observed at 770 – 780 nm was blue shifted to 500 – 700 nm (Fig. 3) [30]. The possible reason for this shift is the lower protonation level of PANI in the nanocomposites when compared to

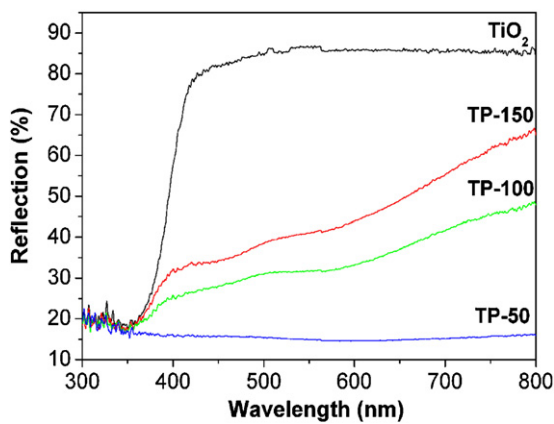


Fig. 3. The UV/vis reflectance spectra of pure TiO_2 and PANI/ TiO_2 nanocomposites.

ordinary PANI-ES [29]. This agrees with the findings of Kohut-Svelko et al. [31] which state that the $\pi \rightarrow$ polaron band shifted toward lower wavelengths as pH increased. The interaction of TiO_2 NPs with PANI chains (possibly *via* hydrogen bonds) may contribute to the presence of deprotonated PANI segments. Another reason for the shifting of the band could be the presence of significant amount of nonordinary segments (structural defects) in the PANI part of the nanocomposites, such as phenazine-like units and chain branching. Such structural defects may increase twisting between aromatic rings, thus leading to the changed electronic structure, *i.e.* increased polaron localization, and to the reduced conjugation length of chains.

As can be seen in Fig. 3, the PANI/ TiO_2 nanocomposites can be activated by UV and visible light simultaneously, which opens the possibility of their application as photocatalysts.

The XRD patterns of TiO_2 NPs and PANI/ TiO_2 nanocomposites are shown in Fig. 4. It can be seen that all the diffraction peaks observed in the XRD pattern of colloidal TiO_2 NPs correspond to the anatase crystalline phase [32,33]. It should be noticed that the diffraction peaks of anatase TiO_2 are relatively broad due to the nanosize of the crystalline particles [32].

In the XRD pattern of PANI/ TiO_2 nanocomposites (Fig. 4) the characteristic peaks of PANI [29] were not detected, due to the fact that the total content of the PANI component was most probably below the detection limit of the XRD technique. Also, it should be considered that the layer of PANI chains adsorbed on the surface of TiO_2 NPs is, most probably, less than 1 nm thick, as was suggested by HRTEM measurements.

Typical TEM images of the TP-100 nanocomposite sample at different magnifications are shown in Fig. 5. The average diameter of the colloidal TiO_2 NPs, used as a precursor for the synthesis

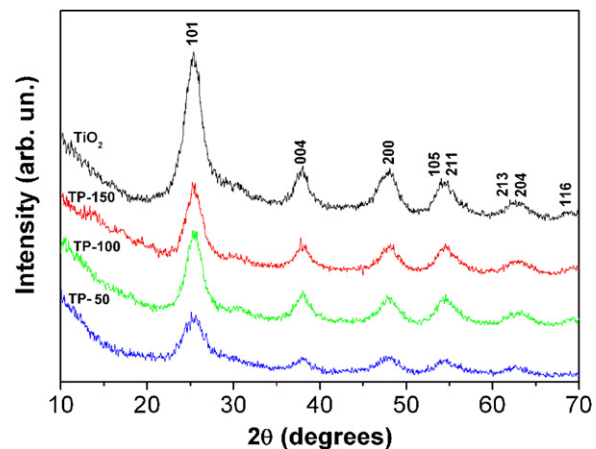


Fig. 4. XRD patterns of bare TiO_2 NPs and PANI/ TiO_2 nanocomposites.

of PANI/ TiO_2 nanocomposites, was 4.5 nm. As can be seen (inset in Fig. 5B), the thickness of the PANI layer uniformly adsorbed on the TiO_2 surface is 0.6–0.7 nm. Considering that the diameter of the benzene structure is 0.5 nm, we assumed that PANI forms monomolecular layered structures on the surface of TiO_2 NPs [34].

3.2. The photocatalytic activity of PANI/ TiO_2 nanocomposites

The photocatalytic degradation of the test (model) molecules MB and RB in the presence of PANI/ TiO_2 nanocomposites under white light irradiation in oxygen atmosphere was studied. The photodegradation of both dyes was followed by concentration changes (C/C_0) as a function of white light illumination time. Kinetic plots of the degradation of MB and RB (the decoloration of the dye solution) are presented in Fig. 6.

The photolysis of both dyes is negligible, less than 1% after 6 h of irradiation. In addition, the degradation of MB and RB in the presence of bare TiO_2 was much slower compared to the degradation in the presence of all the nanocomposites, as can be seen in Fig. 6. The bare TiO_2 NPs removed about 5.5% of MB and about 17% of RB from the solution after 6 h of white light illumination, as was expected, taking into account the fact that UV light (crucial for the activation of TiO_2 NPs) occupies only a small part of the solar spectrum. The synthesized TP-50, TP-100 and TP-150 nanocomposites removed 57, 55 and 20% of MB and 48, 96 and 85% of RB from the solution after 6 h of illumination, respectively. The best photocatalytic activity was observed using TP-50/TP-100 in the case of MB degradation and using TP-100 when RB degradation was studied.

The results can be viewed in different ways, concerning the optical properties of nanocomposites, bearing in mind the mechanism

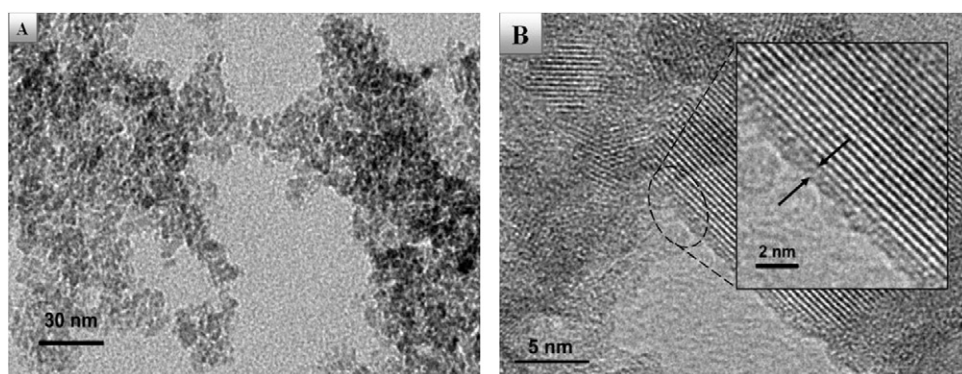


Fig. 5. TEM images of the TP-100 nanocomposite (A and B); inset: higher magnification of (B).

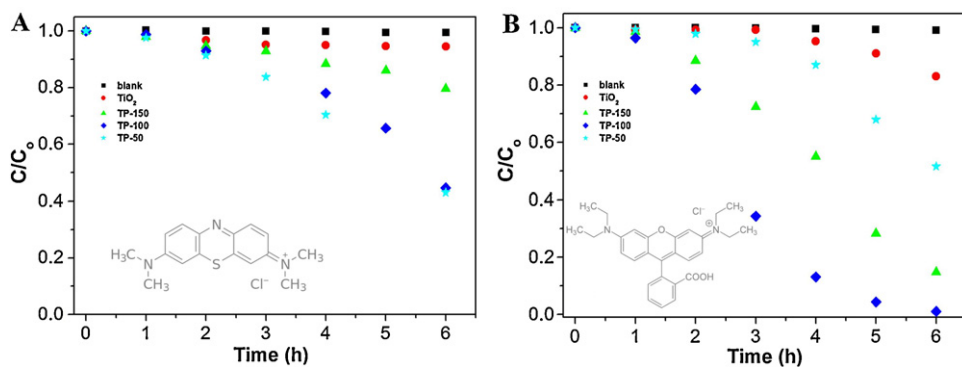


Fig. 6. Kinetic plots of the degradation of MB (A) and RB (B) in the presence of bare TiO_2 NPs and various PANI/ TiO_2 nanocomposites, where C_0 is the initial concentration of dye (obtained after centrifugation of the equilibrated dispersions before irradiation) and C is the concentration of dye at time t . Corresponding plots for dyes solution without the presence of TiO_2 and PANI/ TiO_2 nanocomposite (blank) are also shown. The molecular structures of MB and RB are presented as insets.

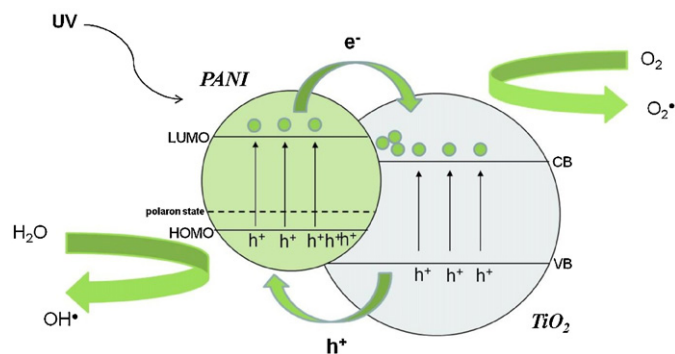


Fig. 7. The mechanism of absorption of the UV component of white light in the presence of the PANI/ TiO_2 nanocomposite (e^- – electron, h^+ – hole).

of light absorption, the molecular structure of dye molecules and the PANI layer in the nanocomposites.

As can be seen in Fig. 3, nanocomposites can absorb visible light to a much greater degree than bare TiO_2 NPs. The possible mechanisms of white light absorption by PANI/ TiO_2 nanocomposites are shown in Figs. 7 and 8 [9,11,35]. The mechanism of absorption of the UV component of white light is presented in Fig. 7.

Under UV-irradiation, both the PANI and TiO_2 absorb photons, and electrons generated by conducting PANI can be transferred into the conduction band of TiO_2 , enhancing the charge separation and the forming of superoxide radicals, in the presence of O_2 . These are consumed in a reaction with water producing OH^\bullet radicals [6,34]. The photogenerated holes in TiO_2 NPs that can migrate to the surface and holes from the PANI species react directly with

the dye molecules to produce $\text{D}^\bullet+$ or indirectly through the OH^\bullet radicals to form degradation products [6,34]. Alternatively, taking into account the position of redox potentials [9,11,35], the holes generated in the valence band of TiO_2 can also migrate to the π -orbital of PANI and make a contribution to the oxidation of adsorbed molecules [6,34].

The mechanism of absorption of the visible component of white light by PANI/ TiO_2 nanocomposites is presented in Fig. 8. Under visible light irradiation of the PANI/ TiO_2 nanocomposites, the transitions $\pi \rightarrow$ polaron and polaron $\rightarrow \pi^*$ in PANI molecules can be induced [30]. Excited-state electrons from the PANI molecules can be injected into the conduction band of TiO_2 and finally react with oxygen at the surface. This results in the formation of highly reactive particles, for example the superoxide radical ion $\text{O}_2^{\bullet-}$ and consequently the hydroxyl radical OH^\bullet . The latter is responsible for the degradation of the organic compound [15]. In this case PANI acts as a photosensitizer.

The photogenerated holes in the π -orbital of PANI can migrate to the interface and react with water to yield hydroxyl radicals. Therefore, the higher photocatalytic activity of this system compared to bare TiO_2 NPs is explained as being due to rapid charge separation and slow charge recombination. However, the increased visible light absorption of the PANI/ TiO_2 nanocomposite is not the only factor that induces increased photocatalytic activity. Comparing results obtained following the degradation of two dye molecules it can be seen that RB is almost completely degraded after 6 h while MB is degraded to only 60% of its initial concentration after the same time.

The TP-50/TP-100 samples showed the best photocatalytic capacity for the degradation of MB. The structure of TP-50 is dominated by the ES form of PANI, according to the Raman spectrum in Fig. 1. We assume that in the TP-50 nanocomposite there must be electrostatic and/or hydrogen bonding interactions between the positively charged PANI-ES chain with delocalized π -electron system (e.g., $-\text{NH}^\bullet+$) and the free electron pair of the nitrogen atom on the MB molecule (Fig. 6A), which allows for a more efficient photocatalytic process in the presence of this sample [36–38]. The worst photocatalytic activity among all nanocomposites was shown by the TP-150 sample. Taking into account the existence of short and branched PANI chains at the expense of PANI-ES segments in this sample, according to Raman spectra, it is logical to expect a reduction in interactions between the polymer chain and the dye molecules, which consequently lead toward the low photocatalytic activity of the TP-150 nanocomposite. The nanocomposite sample TP-100 has in its structure PANI-ES and PANI-EB-like segments and showed a similar level of photoactivity to the TP-50 sample.

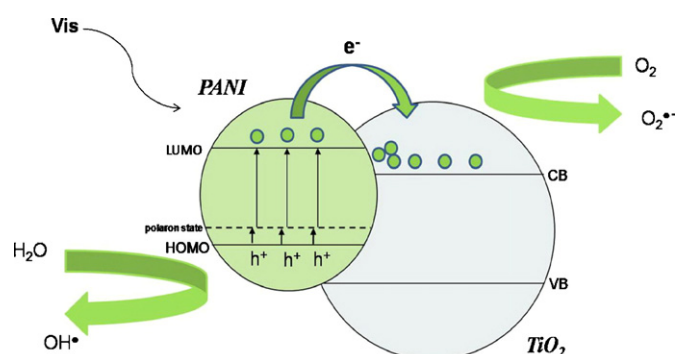


Fig. 8. The mechanism of absorption of the visible component of white light in the presence of the PANI/ TiO_2 nanocomposite.

The photocatalytic activities of PANI/TiO₂ nanocomposites in the process of RB degradation increase as the content of PANI in the nanocomposite increases, with a maximum value for TP-100 and a slight decrease of photocatalytic activity for the TP-150 sample. The reason for this might be found in the possible interaction of RB dyes through carboxyl groups with the surface OH groups of TiO₂ NPs, particularly in the TP-150 nanocomposite sample. On the other hand, in the TP-50 sample, where the PANI-ES form prevails, the approach of RB molecules to the surface of TiO₂ NPs is hindered due to the repulsion between positively charged PANI-ES chains and cationic groups of dye, which leads to its significantly reduced photocatalytic activity.

The optimal photocatalytic activity of the TP-100 nanocomposite sample could be explained by the protonation of PANI-EB form with carboxyl group of RB (Fig. 6B), which leads to the increased electrostatic interaction between PANI chains and dye molecules and consequently to better photocatalytic activity [39,40]. Additionally, OH groups on the TiO₂ NPs surface could easily react with the –COOH group in RB, thus enabling better contact between dye and catalyst.

Bearing in mind obtained results it is clear that the photocatalytic efficiencies of synthesized PANI/TiO₂ nanocomposites (except for the sample TP-50) are generally better in the process of RB degradation compared to the process of MB degradation. Reason for such behavior could be found in the structure of dyes. Regardless of the cationic character of both dyes, more efficient degradation of RB dye (particularly for the samples TP-100 and TP-150) could be explained by the presence of carboxyl group in its structure. Interaction of carboxyl groups with TiO₂ NPs surface and protonation of PANI-EB forms (TP-100) caused increasing of photocatalytic degradation of RB dye molecule. Moreover, it should be taken into account that influence of cationic part of molecule is additionally suppressed by steric hindrance of o-carboxyphenyl group in RB dye molecule.

On the other hand, the difference in surface structure of PANI/TiO₂ photocatalysts (PANI-ES and PANI-EB like forms, short and branched PANI chains) also must be considered. Due to the presence of polaronic and bipolaronic forms, positively charged PANI-ES chains in the sample TP-50 induced repelling between both dye molecules and surface of nanocomposite, which consequently lead toward lower photocatalytic efficiency of this sample in the process of MB and RB degradations. The reason for more efficient RB degradation in the presence of TP-150 nanocomposite could be found in smooth interaction between OH groups on the TiO₂ NPs surface and carboxyl group in RB dye which is facilitated by the presence of smaller amounts of PANI on the TiO₂ surface.

At the end, considering the results obtained, it is clear that the efficiency of synthesized photocatalysts depends on the structures of dyes and the surface of the PANI/TiO₂ nanocomposites, as well as on the mechanism of light absorption of the PANI/TiO₂ nanocomposites. In the framework of our experiments, the best results are obtained for TP-100, following degradation of both dyes, which has an optimal balance between optical absorption and the surface composition/structure of PANI/TiO₂ (PANI-ES and PANI-EB-like forms).

4. Conclusions

In order to improve the photocatalytic activity of TiO₂ NPs, PANI/TiO₂ nanocomposites have been synthesized by *in situ* chemical oxidative polymerization of aniline with APS in colloidal TiO₂ solution without added acid. This was done by using initial TiO₂/aniline mole ratios 50, 100, and 150. Raman spectroscopy confirmed the presence of the PANI-ES form in the TP-50 sample, PANI-ES and PANI-EB-like segments in the TP-100 sample,

and phenazine-type units in all nanocomposites, and indicated branched oligomers in the TP-150 sample. The presence of TiO₂ NPs with anatase crystal structure in PANI/TiO₂ nanocomposites was confirmed by the appearance of characteristic anatase TiO₂ peaks in Raman spectra, as well as by the XRD pattern. A PANI monolayer was formed on the TiO₂ NPs surface according to TEM measurements. PANI/TiO₂ nanocomposites were successfully applied for the degradation of Rhodamine B and Methylene blue using white light. They showed higher photocatalytic efficacy compared to bare TiO₂ NPs. The photocatalytic activity of nanocomposites is strongly influenced by their surface structure and the molecular structures of the organic dyes used.

Acknowledgments

Financial support for this study was granted by The Ministry of Education, Science and Technological Development of The Republic of Serbia, Projects: ON172056, ON172043 and III45020.

References

- [1] A. Fujishima, T.N. Rao, D.A. Tryk, *Journal of Photochemistry and Photobiology C* 1 (2000) 1–21.
- [2] A.L. Linsebigler, G. Lu, J.T. Yates Jr., *Chemical Reviews* 95 (1995) 735–758.
- [3] Y.C. Qiu, W. Chen, S.H. Yang, *Angewandte Chemie International Edition* 49 (2010) 3675–3679.
- [4] D.P. Hagberg, J.H. Yum, H.J. Lee, F.D. Angelis, T. Marinado, K.M. Karlsson, R.H. Baker, L.C. Sun, A. Hagfeldt, M. Gratzel, M.K. Nazeeruddin, *Journal of the American Chemical Society* 130 (2008) 6259–6266.
- [5] X. Chen, S. Mao, *Chemical Reviews* 107 (2007) 2891–2959.
- [6] X. Li, D. Wang, G. Cheng, Q. Luo, J. An, Y. Wang, *Applied Catalysis B: Environmental* 81 (2008) 267–273.
- [7] S.X. Xiong, Q. Wang, H.S. Xia, *Synthetic Metals* 146 (2004) 37–42.
- [8] L.X. Zhang, P. Liu, Z.X. Su, *Polymer Degradation and Stability* 91 (2006) 2213–2219.
- [9] J. Li, L.H. Zhu, Y.H. Wu, Y. Harima, A.Q. Zhang, H.Q. Tang, *Polymer* 47 (2006) 7361–7367.
- [10] F. Wang, S. Min, Y.H.L. Feng, *Superlattices and Microstructures* 48 (2010) 170–180.
- [11] J. Yue, Z.H. Wang, K.R. Cromack, A.J. Epstein, A.G. MacDiarmid, *Journal of the American Chemical Society* 113 (1991) 2665–2671.
- [12] S. Min, F. Wang, Y. Han, *Journal of Materials Science* 42 (2007) 9966–9972.
- [13] F. Wang, S.X. Min, *Chinese Chemical Letters* 18 (2007) 1273–1277.
- [14] X.Y. Li, D.S. Wang, Q.Z. Luo, J. An, Y.H. Wang, G.X. Cheng, *Journal of Chemical Technology and Biotechnology* 83 (2008) 1558–1564.
- [15] Q. Yu, M. Wang, H. Chen, Z. Dai, *Materials Chemistry and Physics* 129 (2011) 666–672.
- [16] L. Gu, J. Wang, R. Qi, X. Wang, P. Xu, X. Han, *Journal of Molecular Catalysis A* 357 (2012) 19–25.
- [17] Y. Wang, J. Xu, W. Zong, Y. Zhu, *Journal of Solid State Chemistry* 184 (2011) 1433–1438.
- [18] D. Mahanta, U. Manna, G. Madras, S. Patil, *ACS Applied Materials and Interfaces* 3 (2011) 84–92.
- [19] T. Rajh, D. Tiede, M. Thurnauer, *Journal of Non-Crystalline Solids* 207 (1996) 815–820.
- [20] R. Thompson, *Inorganic Chemistry* 23 (1984) 1794–1798.
- [21] M. Radoičić, Z. Šaponjić, J. Nedeljković, G. Čirić-Marjanović, J. Stejskal, *Synthetic Metals* 160 (2010) 1325–1334.
- [22] N.T. Nolan, M.K. Seery, S.C. Pillai, *Journal of Physical Chemistry C* 113 (2009) 16151–16157.
- [23] H.C. Choi, Y.M. Jung, S.B. Kim, *Vibrational Spectroscopy* 37 (2005) 33–38.
- [24] G. Čirić-Marjanović, M. Trchová, J. Stejskal, *Journal of Raman Spectroscopy* 39 (2008) 1375–1380.
- [25] M. Trchová, I. Šeděnková, E.N. Konyushenko, J. Stejskal, P. Holler, G. Čirić-Marjanović, *Journal of Physical Chemistry B* 110 (2006) 9461–9468.
- [26] G. Čirić-Marjanović, M. Trchová, J. Stejskal, *Collection of Czechoslovak Chemical Communications* 71 (2006) 1407–1426.
- [27] G. Čirić-Marjanović, M. Trchová, J. Stejskal, *International Journal of Quantum Chemistry* 108 (2008) 318–333.
- [28] G. Čirić-Marjanović, M. Trchová, E.N. Konyushenko, P. Holler, J. Stejskal, *Journal of Physical Chemistry B* 112 (2008) 6976–6987.
- [29] M. Radoičić, Z. Šaponjić, G. Čirić-Marjanović, Z. Konstantinović, M. Mitić, J. Nedeljković, *Polymer Composites* 33 (2012) 1482–1493.
- [30] Y. Xia, J.M. Wiesinger, A.G. MacDiarmid, *Chemistry of Materials* 7 (1995) 443–445.
- [31] N. Kohut-Svelko, S. Reynaud, J. Francois, *Synthetic Metals* 150 (2005) 107–114.
- [32] N.D. Abazović, M.I. Čomor, M.D. Dramićanin, D.J. Jovanović, S.P. Ahrenkiel, J.M. Nedeljković, *Journal of Physical Chemistry B* 110 (2006) 25366–25370.
- [33] N.D. Abazović, I.A. Ruvarac-Bugarčić, M.I. Čomor, N. Babić, S.P. Ahrenkiel, J.M. Nedeljković, *Optical Materials* 30 (2008) 1139–1144.

- [34] H. Zhang, R. Zong, J. Zhao, Y. Zhu, *Environmental Science and Technology* 42 (2008) 3803–3807.
- [35] G.K.R. Senadeera, T. Kitamura, Y. Wadab, S. Yanagida, *Journal of Photochemistry and Photobiology A* 164 (2004) 61–66.
- [36] Y. Tang, B.L. Allen, D.R. Kauffman, A. Star, *Journal of the American Chemical Society* 131 (2009) 13200–13201.
- [37] Z. Liu, C. Zhang, L. Luo, Z. Chang, X. Sun, *Journal of Materials Science* 22 (2012) 12149–12154.
- [38] S.M. Bakalova, L.M. Frutos, J. Kaneti, O. Castano, *Journal of Physical Chemistry A* 109 (109) (2005) 10388–10395.
- [39] C.A. Amarnath, S. Palaniappan, *Polymers for Advanced Technologies* 16 (2005) 420–424.
- [40] A. Janošević, G. Ćirić-Marjanović, M. Trchová, B. Marjanović, J. Stejskal, *Materials Letters* 64 (2010) 2337–2340.